Supporting Information

Twist et al. 10.1073/pnas.1113328108

SI Materials and Methods

Strains and Plasmids. A complete list of strains and plasmids is provided in Table S3.

Protein Expression and Purification. The T4 *gp33* gene and an *Eco rpoB* gene fragment encoding the β-flap (amino acids 831–1,057) were cloned as a single operon (Fig. S1*A*) in a modified pET28a (Novagen) vector (1) and coexpressed in BL21(DE3) cells that were induced with 0.5 mM isopropyl β-d-thiogalactopyranoside (IPTG) for 16 h at 16 °C. Gp33 was expressed with an N-terminal PreScission Protease (GE Healthcare) cleavable His_6-tag; post-cleavage the gp33 protein has an additional three N-terminal residues GPH. The complex was purified by: Ni^{2+}-affinity chromatography, removal of the His_6-tag and uncleaved complex by subtractive Ni^{2+}-affinity chromatogray, and size-exclusion chromatography (Fig. S1*A*). The SeMet-substituted proteins (2) were produced by suppression of endogenous methionine biosynthesis (3) and purified as described for the native proteins. Purified complex was dialyzed into storage buffer (10 mM Tris pH 8.0, 150 mM NaCl, 1% glycerol, 1 mM β-mercaptoethanol, 1 mM DTT).

Crystallization and Structure Determination. Crystals were grown by hanging-drop vapor diffusion at 22 °C. The native complex was crystallized by mixing 1 μL:1 μL of protein solution (7.5–12 mg/mL) with reservoir solution (0.1 M Tris pH 8.5, 0.1 M triethylamine N-oxide, 20% polyethylene glycol 2,000 monomethylether). The crystals were cryoprotected by slow exchange of the crystallization solution with 0.1 M triethylamine N-oxide, 23% polyethylene glycol 2,000 monomethylether, 20% ethylene glycol and subsequent flash-freezing in liquid nitrogen. The SeMet-complex was similarly crystallized above a reservoir solution of 0.2 M tri-Potassium citrate, 20% (wt/vol) polyethylene glycol 3350, and cryoprotected in a like manner in a cryosolution of 0.2 M tripotassium citrate, 25% (wt/vol) polyethylene glycol 3350, 20% ethylene glycol. These two sets of crystals were isomorphous and belonged to the orthorhombic space group *I*222, with 67% solvent content and one molecule of each protein/asymmetric unit. Full datasets for each of the native and SeMet-complexes were collected from single crystals at beamline X3A, National Synchrotron Light Source, Brookhaven National Laboratory. The native crystals diffracted to 3.1 Å-resolution, and the SeMet-crystals diffracted to 3.0 Å-resolution. The data were processed using HKL2000 (4). Initial phases were obtained by molecular replacement [PHASER (5)] using a homology model of the *Eco* β-flap [built using MODELLER (6)] based on the *Taq* core RNAP crystal structure (7) as a template. However, the resulting maps did not have clear density for the gp33 protein. In addition, experimental phases were derived from single-wavelength anomalous dispersion (SAD) phasing from the SeMet data. Four of the five possible Se sites were located using anomalous difference Fourier maps with the molecular replacement phases. SAD phases were calculated using SHARP (8). Combining the SAD phases with the molecular replacement phases did not substantially improve the electron density maps, so the SAD phases alone were used for the initial experimental maps, which were improved by density modification using CNS (9). The model was manually built and refined against the SeMet-amplitudes in iterative steps using COOT (10) and Refmac5 (11).

Creation of T4 Late Promoter Open Complex Model. To create a model of a T4 late gene promoter open complex, we started with a *Taq* RNAP open complex model derived from Murakami et al. (12). Gp55 is represented by conserved regions 1.2 and 2 of *Taq* σ^A (residues 93–111 and 203–278) and the rest of σ^A was deleted. We then replaced *Taq* core with the recently described homology model of *Eco* RNAP (PDB ID 3LU0) (13). Next, the β-flap module was replaced by the gp33/β-flap crystal structure by aligning β-flap-wall residues (*Eco* β-subunit residues 831–890, 913–937, and 1,043–1,057). The DNA upstream of the −10 element was replaced with straight, B-form DNA, and the path was altered to alleviate clashes with gp33 (because gp33, unlike $\sigma^A{}_4$, is not known to interact with DNA). To add the sliding-clamp gp45 to the model, we first took the structure of the *Eco* β clamp with DNA [PDB ID 3BEP; (14)] and aligned it onto the structure of the sliding-clamp of phage RB69 (a close homolog of T4) bound to the DNA polymerase SCBM [PDB 1B8H (15)] to make a composite model of the RB69 sliding-clamp bound to both an SCBM and to DNA. The DNA in the RB69/DNA model was then aligned with the upstream DNA of the open complex model (with the SCBM-binding face of the sliding-clamp facing RNAP) and then the clamp with DNA was moved in the downstream direction (toward RNAP) one bp at a time until it was as close as possible without severe steric clashes.

The model contains ambiguities in several details: (*i*) It is constructed with the closed-ring conformation of its sliding-clamp, but there is evidence that the T4 sliding-clamp assumes an out-of-plane open conformation, even when mounted on DNA (16, 17), (*ii*) It follows the structure in ref. 15 in attaching the gp33 SCBD to a hydrophobic patch that each subunit of DNA-mounted gp45 presents to the upstream-facing end of RNAP. Similar binding sites are ubiquitously presented by sliding clamps to their ligands (18). On the contrary, the T4 SCBD is demonstrated to bind preferentially to the intersubunit cleft of the T4 sliding-clamp in solution (16, 17). These ambiguities prevent us from specifying the rotational setting of the sliding-clamp in the promoter complex, although it is likely that gp33 binding fixes a well defined orientation, and from exploring the likely existence of additional sites of sliding-clamp/RNAP interaction, and (*iii*) The model also does not specify the attachment site of the gp55 SCBD; the evidence at hand (19) suggests that, in contrast to gp33, the gp55 SCBD is flexibly linked to the body of this protein.

β-Galactosidase Assays. For the bacterial two-hybrid assays FW102 O_L2-62 reporter strain cells were cotransformed with the indicated pAC and pBR derived plasmids (Table S3). Individual transformants were selected and grown in LB supplemented with carbenicillin (50 μg/mL), chloramphenicol (25 μg/mL), kanamycin (50 μg/mL) and the specified concentration of IPTG. β-galactosidase assays were performed as described (20) using microtiter plates and a microtiter plate reader. Miller Units were calculated as described (20).

1. Campbell EA, Darst SA (2000) The anti-σ factor SpoIIAB forms a 2:1 complex with σ^F, contacting multiple conserved regions of the σ factor. *J Mol Biol* 300:17–28.
2. Hendrickson W, Norton JR, LeMaster DM (1990) Selenomethionyl proteins produced for analysis by multiwavelength anomalous diffraction (MAD). *EMBO J* 9:1665–1672.
3. Doublie S (1997) Preparation of selenomethionyl proteins for phase determination. *Methods Enzymol* 276:523–530.
4. Otwinowski Z, Minor W (1997) Processing of X-ray diffraction data collected in oscillation mode. *Methods Enzymol* 276:307–326.
5. McCoy AJ, et al. (2007) Phaser crystallographic software. *J Appl Crystall* 40:658–674.

6. Sali A, Blundell TL (1993) Comparative protein modelling by satisfaction of spatial restraints. *J Mol Biol* 234:779–815.
7. Zhang G, et al. (1999) Crystal structure of *Thermus aquaticus* core RNA polymerase at 3.3 Å resolution. *Cell* 98:811–824.
8. de La Fortelle E, Irwin JJ, Bricogne G (1997) SHARP: A maximum-likelihood heavy-atom parameter refinement and phasing program for the MIR and MAD methods. *Crystallographic Computing*, eds Bourne P, Watenpaugh K (Kluwer Academic Publishers, Boston), Vol 7, pp 1–9.
9. Adams PD, Pannu NS, Read RJ, Brunger AT (1997) Cross-validated maximum likelihood enhances crystallographic simulated annealing refinement. *Proc Natl Acad Sci USA* 94:5018–5023.
10. Emsley P, Cowtan K (2004) COOT: model-building tools for molecular graphics. *Acta Crystallogr D Biol Crystallogr* 60:2126–2132.
11. Murshudov GN, Vagin AA, Dodson EJ (1997) Refinement of macromolecular structures by the maximum-likelihood method. *Acta Crystallogr D Biol Crystallogr* D53:240–255.
12. Murakami K, Masuda S, Campbell EA, Muzzin O, Darst SA (2002) Structural basis of transcription initiation: An RNA polymerase holoenzyme/DNA complex. *Science* 296:1285–1290.
13. Opalka N, et al. (2010) Complete structural model of *Escherichia coli* RNA polymerase from a hybrid approach. *PLoS Biol.* 8:e1000483.
14. Georgescu RE, et al. (2008) Structure of a sliding-clamp on DNA. *Cell* 132:43–54.
15. Shamoo Y, Steitz TA (1999) Building a replisome from interacting pieces: sliding-clamp complexed to a peptide from DNA polymerase and a polymerase editing complex. *Cell* 99:155–166.
16. Millar D, Trakselis MA, Benkovic SJ (2004) On the solution structure of the T4 sliding-clamp. *Biochemistry* 43:12723–12727.
17. Trakselis MA, Alley SC, Abel-Santos E, Benkovic SJ (2001) Creating a dynamic picture of the sliding-clamp during T4 DNA polymerase holoenzyme assembly by using fluorescence resonance energy transfer. *Proc Natl Acad Sci USA* 98:8368–8375.
18. Indiani C, O'Donnell M (2006) The replication clamp-loading machine at work in the three domains of life. *Nat Rev Mol Cell Biol* 7:751–761.
19. Nechaev S, Geiduschek EP (2008) Dissection of the bacteriophage T4 late promoter complex. *J Mol Biol* 379:402–413.
20. Nickels BE (2009) Genetic assays to define and characterize protein-protein interactions involved in gene regulation. *Methods* 47:53–62.

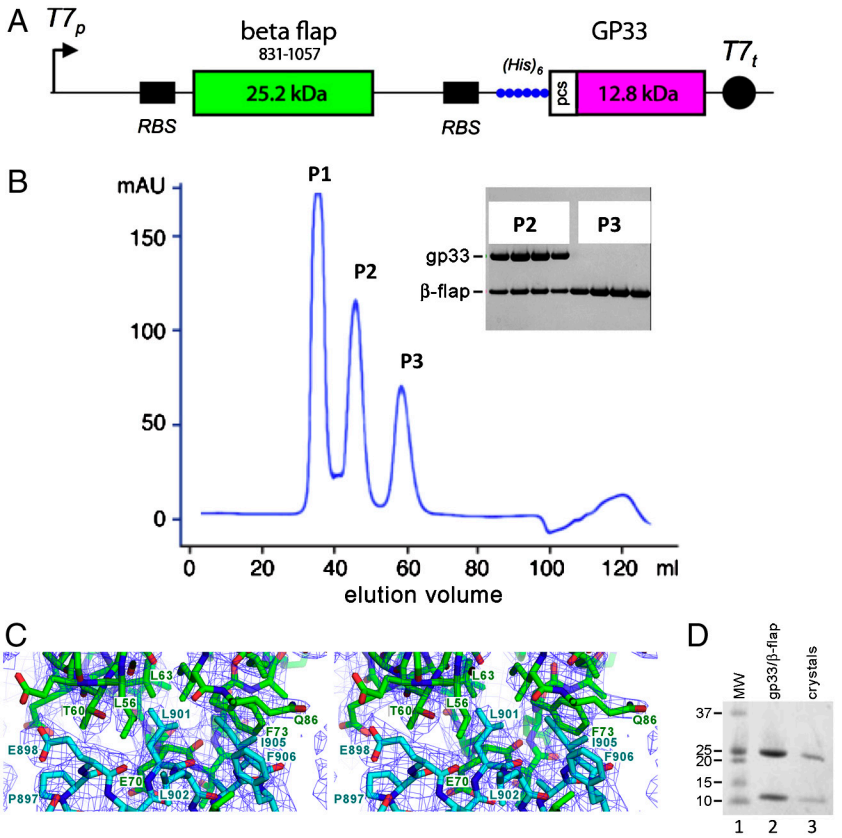

Fig. S1. Purification, crystallization, and structure determination of the gp33/β-flap complex. (*A*). The expression construct used to coexpress gp33 and the β-flap is shown in schematic. Abbreviations: pcs PreScission Protease (GE healthcare) cleavage site; RBS, ribosomal binding site; T7p, T7 promoter; T7t, T7 terminator. (*B*). Chromatogram from size-exclusion chromatography (Superdex 75, GE Healthcare) of the complex. Fractions containing the peaks P2 and P3 were analyzed by SDS-PAGE and visualized by Coomassie staining (inset; P1 did not contain protein and eluted in the void volume). P2 shows the stable, 1:1 complex. P3 contains excess free gp33. (*C*). Experimental electron density map. Stereo view of the experimental electron density map, contoured at 1σ. The final model is shown as sticks and colored according to Fig. 1. Nitrogen and oxygen atoms are colored blue and red, respectively. Shown is the gp33/β-FTH interaction, with interacting residues labeled (see Fig. 2 *A* and *B*). (*D*). The crystals contain full-length gp33 and β-flap module proteins. Lanes: 1, molecular weight markers with weight (kDa) shown on left; 2, purified proteins as crystallized; 3, washed, dissolved crystals.

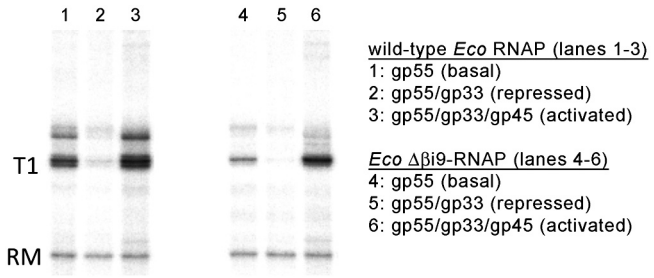

Fig. S2. The βi9 (β-subunit dispensable region 2 or DR2) is not involved in gp33 function: a comparison of basal, repressed, and activated single-round T4 late transcription with wild-type *Eco* RNAP and *Eco* RNAP bearing a deletion of βi9 (β residues 967–1,028; Δβi9-RNAP). The transcript terminating at T1, the first *rrnB* terminator and the recovery marker (RM) are shown. The Δβi9-RNAP is less active (compare lanes 1 and 4), but is fully repressed by gp33 (compare lanes 2 and 5), and normally activated by gp45 (compare lanes 3 and 6). Method: Reaction mixtures contained, in 15 μL, 100 fmol DNA, 1 pmol (by weight) RNAP, 6 pmol each of gp55, gp33 (as indicated) and gp45 trimer (as indicated), 2.4 pmol gp44/62 complex (clamp loader), and 15 pmol gp32 (single-stranded-DNA-binding protein) in Transcription Buffer (33 mM Tris acetate, pH 7.8, 10 mM Mg-acetate, 200 mM K-acetate, 1 mM DTT, 150 μg/mL BSA). The DNA was the previously described linear template comprising a T4 late transcription unit consisting of the gene 23 promoter upstream of two *rrnB* terminators, with a downstream sliding-clamp-loading site generated by recessing the nontranscribed (nontemplate) strand 3′-end by ∼100 nt (19). DNA, gp32 and gp44/62 complex, in 7.5 μL Transcription Buffer, were added to RNAP core, gp33 (as indicated), gp55, gp45 (as indicated) and 15 nmol dATP, in 7.5 μL Transcription Buffer, and equilibrated for 5 min at 25 °C (allowing for sliding-clamp-loading and promoter opening). A single round of transcription was generated by adding 20 nmol each of ATP and GTP, 1 nmol each of CTP and $(\alpha\text{-}^{32}\text{P})$UTP, 4.5U RNAguard and 2 μg heparin in 5 μL Transcription Buffer, and was terminated after 6 min by adding 180 μL of Stop Solution (40 mM Tris Cl, pH 8.0, 20 mM EDTA, 0.04% (wt/vol) SDS) containing 74-nt ^{32}P-labeled DNA recovery marker.

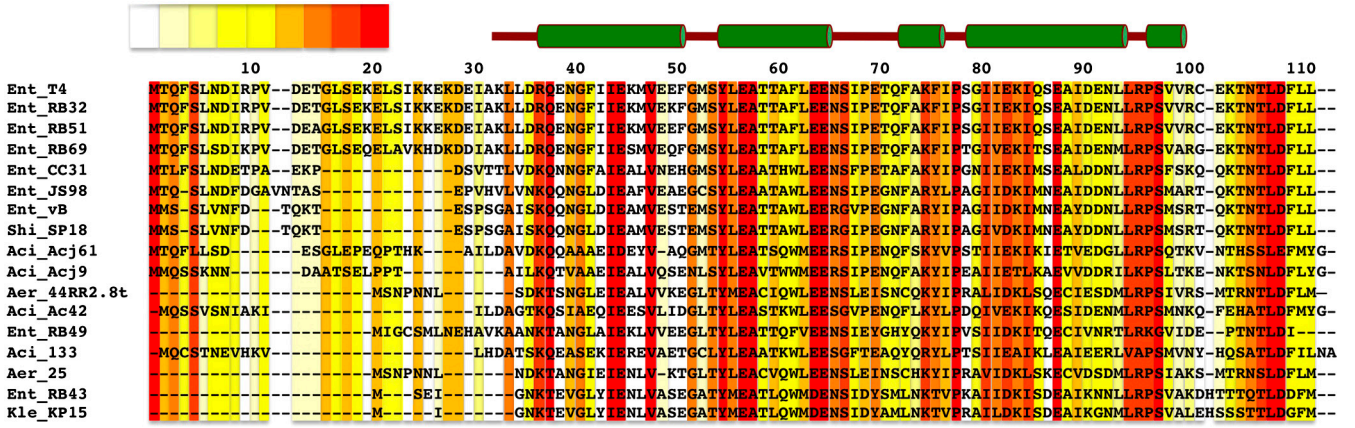

Fig. S3. An alignment of gp33 homologs from the T4 bacteriophage group is color-coded according to conservation score [red, highest identity (1)]. The host bacterial genus and phage encoding each gp33 homolog are listed to the left of the alignment with the following nomenclature: bacteria_phage. Bacterial genera are abbreviated as: *Ent* (Enterobacteria), *Shi* (Shigella), *Aci* (Acinetobacter), *Aer* (Aeromonas) and *Kle* (*Klebsie*lla).

1 Landau M, et al. (2005) ConSurf 2005: the projection of evolutionary conservation scores of residues on protein structures. *Nucleic Acids Res* 33:W299–W302.

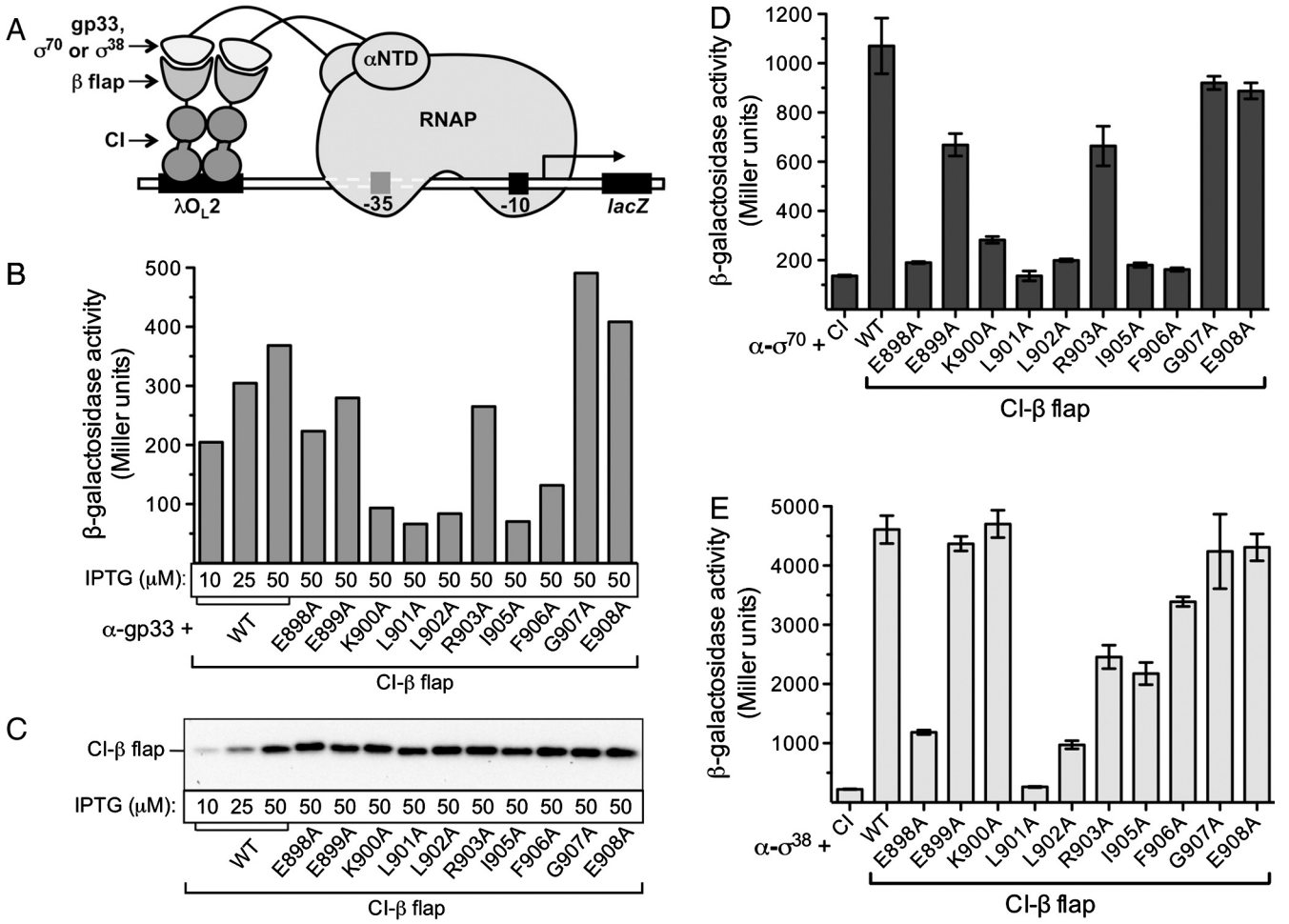

Fig. S4. Use of the bacterial two-hybrid assay to test the effects of alanine substitutions at β flap residues 898–908 (except position A904) on the gp33/β-flap, $\sigma^{70}{}_4/\beta$-flap and $\sigma^{38}{}_4/\beta$-flap interactions. (*A*). Cartoon depicts how the interaction between gp33, $\sigma^{70}{}_4$ or $\sigma^{38}{}_4$ (fused to the α-NTD) and the β-flap (fused to the bacteriophage λCI protein) activates transcription from test promoter p*lac*O_L2-62, which bears the λ operator O_L2 centered 62 bp upstream of the start site of the *lac* core promoter. In reporter strain FW102 O_L2-62, test promoter p*lac*O_L2-62 is located on an F′ episome and upstream of a *lacZ* reporter gene. (*B*). The bacterial two-hybrid assay was used to show that alanine substitutions at β-flap residues 900, 901, 902, 905, 906 disrupt the gp33/β-flap interaction. To control for any possible differences in the intracellular concentrations of the wild-type and mutant λCI-β-flap fusion proteins, the assay was performed in the presence of the indicated concentrations of IPTG and protein samples were collected from the same cells for analysis of intracellular fusion protein levels by Western blotting [shown in (*C*)]. The results of β-galactosidase assays are shown. (*C*). Western blot showing λCI-β-flap fusion protein levels from the same cells as in (*B*). Normalized samples of lysates from (*B*) were processed for Western blotting and the wild-type and mutant λCI-β flap fusion proteins were detected with an anti-λCI antibody (generous gift from J. Beckwith). The blot shows that the intracellular levels of the wild-type and mutant fusion proteins at 50 μM IPTG were equivalent and significantly higher than the intracellular levels of the wild-type fusion protein at either 10 or 25 μM IPTG. Because the β-galactosidase levels measured in cells containing the wild-type λCI-β-flap fusion protein (in the presence of the α-gp33 fusion protein) were higher at 25 or 10 μM IPTG than the β-galactosidase levels measured in cells containing the mutant λCI-β flap fusion proteins (K900A, L901A, L902A, I905A and F906A) at 50 μM IPTG, we conclude that even subtle differences in the intracellular concentrations of the various λCI-β flap fusion proteins cannot account for the failure of the mutant λCI-β flap fusion proteins to activate transcription from the two-hybrid test promoter. We conclude, rather, that substitutions at these positions weaken the gp33/β-flap interaction. (*D*, *E*). Use of the bacterial two-hybrid assay to test the effects of alanine substitutions at β-flap residues 898-908 (except A904) on the $\sigma^{70}{}_4/\beta$-flap interaction (*D*) and the $\sigma^{38}{}_4/\beta$-flap interaction (*E*). Results of β-galactosidase assays performed with reporter strain cells containing one plasmid that encodes the α-$\sigma^{70}{}_4$ protein (*D*) or α-$\sigma^{38}{}_4$ protein (*E*) and a compatible plasmid that encodes either λCI or the indicated λCI-β-flap variant. The plasmids directed the synthesis of the fusion proteins under the control of IPTG-inducible promoters and the cells were grown in the presence of 50 μM IPTG (*D*) or 25 μM IPTG (*E*). The bar graph shows the averages of three independent measurements and standard deviations.

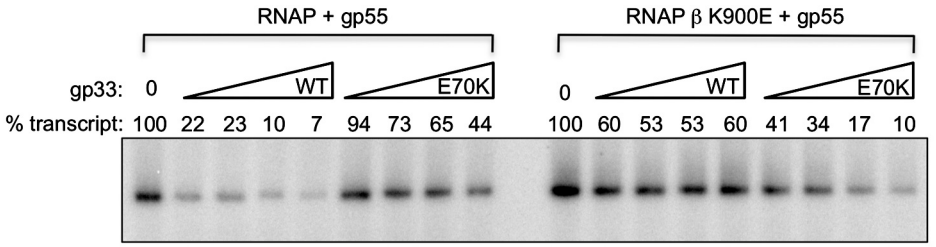

Fig. S5. Gp33 repression assay. In the presence of the wild-type RNAP holoenzyme, wild-type gp33 repressed basal transcription from the gp55-dependent P23 promoter more efficiently than did gp33-E70K, whereas in the presence of the RNAP β-K900E holoenzyme, gp33-E70K repressed basal transcription more efficiently than did wild-type gp33. Wild-type RNAP and mutant RNAP β-K900E core enzymes were purified as described (1). Gp55, gp33 and gp33-E70K were purified as described (2). The 230 bp linear DNA template, which was PCR-amplified from plasmid pGp23_t_r' (Table S3), harbors the T4 gene 23 late promoter (bp −32 to +1) upstream of transcription terminator t_r' and directs the synthesis of a 117 bp transcript. Wild-type or mutant RNAP core (20 nM), gp55 (240 nM) and 0, 30, 60, 120 or 240 nM gp33 or gp33-E70K as indicated, were incubated with 10 nM DNA template for 20 min at 37 °C in transcription buffer (20 mM Tris-HCl [pH 8.0], 0.1 mM EDTA, 50 mM KCl, 100 μg/mL BSA, 10 mM DTT) containing 200 μM GTP, ATP and CTP and 50 μM UTP (supplemented with 1 μCi/μL [α-^{32}P]-UTP). A single-round of transcription was initiated by adding 4 mM $MgCl_2$ and 10 μg/ml rifampicin. Reactions were stopped after 5 min and RNA transcripts were separated by electrophoresis on a 12% denaturing polyacrylamide sequencing gel, visualized by PhosphorImagery, and analyzed using ImageQuant software. Above the gel is shown the percentage of transcripts obtained in the presence of gp33 or gp33-E70K for each holoenzyme, compared to that obtained in the absence of gp33 for each holoenzyme, which was set to 100%. The experiment was repeated three times with similar results.

1 Deighan P, Diez CM, Leibman M, Hochschild A, Nickels BE (2008) The bacteriophage lambda Q antiterminator protein contacts the beta-flap domain of RNA polymerase. *Proc Natl Acad Sci USA* 105:15305–15310.105:15305–15310.
2 Kolesky S, Ouhammouch M, Brody EN, Geiduschek EP (1999) Sigma competition: the contest between bacteriophage T4 middle and late transcription. *J Mol Biol* 291:267–281.

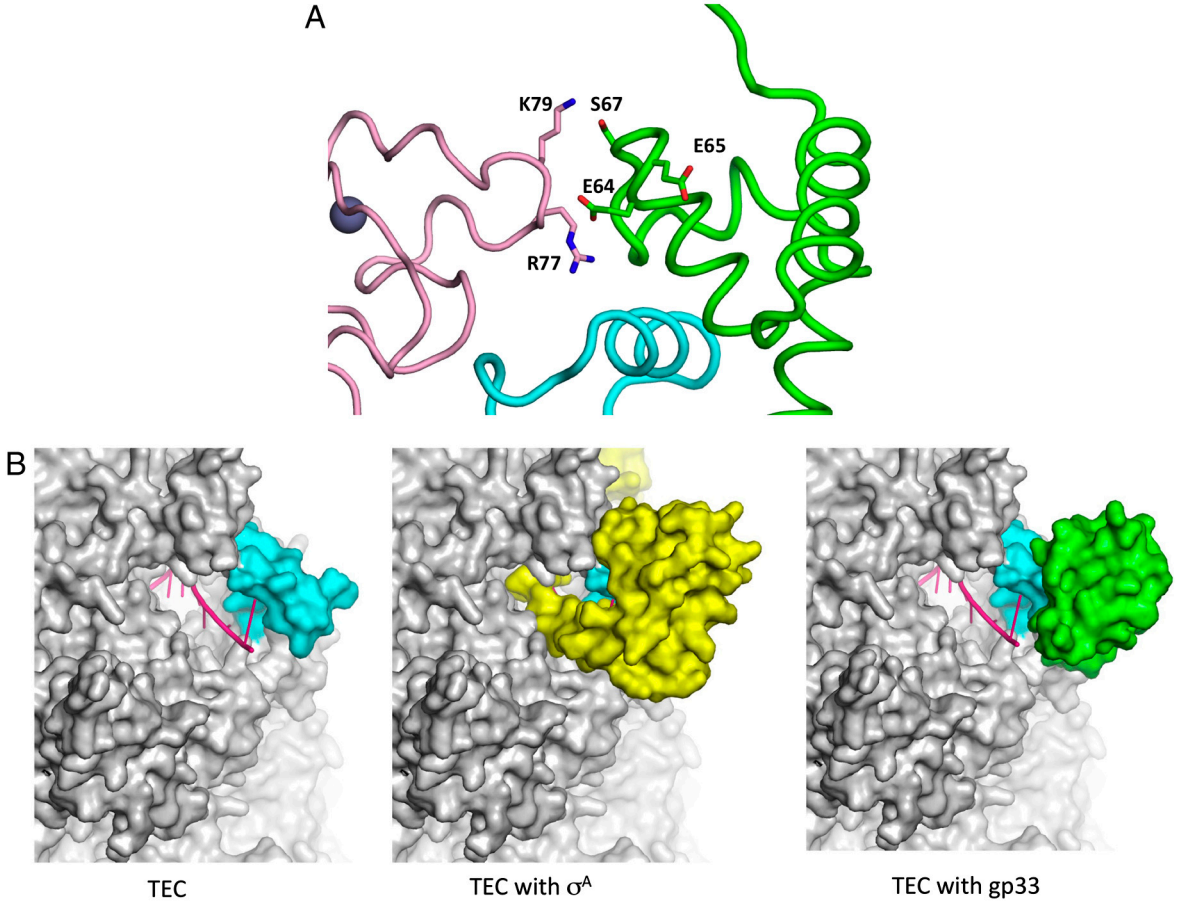

Fig. S6. Distinctive aspects of gp33- and σ_4-bound RNAP. (*A*). Close-up view of predicted interactions between the β′-ZBD (pink, with Zn^{2+} shown as a gray sphere) and residues of conserved patch P4 of gp33 (green). The β-flap (cyan) is also shown. (*B*). Elongation complexes. (left) RNA (magenta cartoon) emerging from the RNA exit channel, formed by the β-flap (colored blue) is unobstructed in the bacterial RNAP TEC structure (1). (middle) The $\sigma_{3.2}$ and σ_4 (yellow) obstruct the path of emerging RNA. (right) The β-flap-bound gp33 (green) does not obstruct the path of emerging RNA.

1 Vassylyev DG, Vassylyeva MN, Perederina A, Tahirov TH, Artsimovitch I (2007) Structural basis for transcription elongation by bacterial RNA polymerase. *Nature* 448:157–162.

Table S1. Crystallographic statistics for *Eco* RNAP βflap-βi9 crystals*

	Nat	Se†
Data collection		
Space group	I222	I222
Cell dimensions		
a, *b*, *c* (Å)	54.70, 110.19, 164.72	55.22, 112.25, 164.85
α, β, γ (°)	90, 90, 90	90, 90, 90
		Peak
Wavelength	0.9785	0.9785
Resolution (Å)	30.0-3.00 (3.11-3.00)	30.0-3.00 (3.11-3.00)
R_{sym}	0.058 (0.57)	0.053 (0.412)
$I/\sigma I$	25.0 (1.7)	21.9 (2.6)
Completeness (%)	89.8 (79.8)	98.1 (93.6)
Redundancy	4.2 (3.0)	3.0 (2.7)
Refinement		
Resolution (Å)		30.0-3.00
No. reflections		9,980
R_{work}/R_{free}		0.264/0.291
No. atoms		
Protein		2,325
Water		0
B-factors		
Protein		29.34
rms deviations		
Bond lengths (Å)		0.008
Bond angles (°)		1.108

*Published previously as Table S1 in ref. 13.
†Scaling statistics for Se1 dataset calculated without combining anomalous pairs.

Table S2. Surface-exposed patches of conserved residues on gp33

Patch*	gp33 residues	function
P1	L95/R96/P97/S98	• interactions with β-flap†
P2	L56/I82/I85	• interactions with β-FTH (L56)†
P3	E57	• putative interaction with β′[395-403].
P4	E64/E65/N66/S67	• putative interaction with β′-ZBD‡
P5	E45/V48/Y55/K84/E88	• faces sliding-clamp in T4 late promoter initiation complex model§. • E45/K84/Y55/E88—likely important for stabilizing the gp33 tertiary structure.
P6	R37/Q38/K75	• creates basic-spot that approaches upstream DNA in T4 late promoter initiation complex model¶

*See Fig. 2*A*.
†See Fig. 3 *A* and *B*.
‡See Fig. S5*A*.
§See Fig. 4.
¶See Fig. 2*C*.

Table S3. Strains and plasmids used in this study

Strains	Relevant details	Reference/source
FW102 O_L2-62	FW102 containing an F′ Kan bearing the p*lac*O_L2-62-*lacZ* fusion where the λCI operator is centered at position −62 upstream of the *lac* promoter	1
Plasmids	**relevant details**	**reference/source**
pACλCI	p*lacUV5*-directed synthesis of the λCI protein	2
pACλCI-β-flap	p*lacUV5*-directed synthesis of the λCI protein fused via three alanines to residues 858–946 of the β subunit of *E. coli* RNAP	3
pACλCI-β-flap E898A	pACλCI-β-flap encoding the E898A substitution in the β moiety of the fusion	4
pACλCI-β-flap E899A	pACλCI-β-flap encoding the E899A substitution in the β moiety of the fusion	4
pACλCI-β-flap K900A	pACλCI-β-flap encoding the K900A substitution in the β moiety of the fusion	4
pACλCI-β-flap K900E	pACλCI-β-flap encoding the K900E substitution in the β moiety of the fusion	this work
pACλCI-β-flap L901A	pACλCI-β-flap encoding the L901A substitution in the β moiety of the fusion	4
pACλCI-β-flap L902A	pACλCI-β-flap encoding the L902A substitution in the β moiety of the fusion	4
pACλCI-β-flap R903A	pACλCI-β-flap encoding the R903A substitution in the β moiety of the fusion	4
pACλCI-β-flap I905A	pACλCI-β-flap encoding the I905A substitution in the β moiety of the fusion	4
pACλCI-β-flap F906A	pACλCI-β-flap encoding the F906A substitution in the β moiety of the fusion	4
pACλCI-β-flap G907A	pACλCI-β-flap encoding the G907A substitution in the β moiety of the fusion	4
pACλCI-β-flap E908A	pACλCI-β-flap encoding the E908A substitution in the β moiety of the fusion	4
pBRα-gp33 E70K	pBN2657 encoding the E70K substitution in the gp33 moiety of the fusion	this work
pBRα-σ38	p*lacUV5*/p*lpp*-directed synthesis of the αNTD fused to σ^{38} region 4 (residues 243–330 of σ^{38})	5
pBRα-σ70 D581G	p*lacUV5*/p*lpp*-directed synthesis of the αNTD (residues 1–248 of the α) fused directly to σ^{70} region 4 (residues 528–613 of σ^{70}). The σ^{70} moiety also carries the D581G substitution	3
pBN2653	p*lacUV5*-directed synthesis of the λCI protein fused via three alanines to gp33	Gift of B. Nickels
pBN2657	p*lacUV5*/p*lpp*-directed synthesis of the αNTD (residues 1–248 of the α) fused via three alanines to gp33	Gift of B. Nickels
pGp23_tr′	Source of template for gp33 in vitro transcription repression assay. pFW11tet with T4 gene 23 late promoter (bp −32 to +1) upstream of transcription terminator t_r'	this work
pIA679	*E. coli* RNAP core subunits overexpression vector. p*T7*-dircted synthesis of *rpoA*, His_6-*rpoB, rpoC, rpoZ*	Gift of I. Artsimovitch
pIA679 His_6-rpoB K900E	p*T7*-directed synthesis of *rpoA*, His_6-*rpoB K900E, rpoC, rpoZ*	this work

1 Deaconescu AM, Chambers AL, Smith AJ, Nickels BE, Hochschild A, Savery NJ, Darst SA (2006) Structural basis for bacterial transcription-coupled DNA repair. *Cell* 124:507–520.
2 Dove SL, Joung JK, Hochschild A (1997) Activation of prokaryotic transcription through arbitrary protein-protein contacts. *Nature* 386:627–630.
3 Kuznedelov K, Minakhin L, Niedziela-Majka A, Dove SL, Rogulja D, Nickels BE, Hochschild A, Heyduk T, Severinov K (2002) A role for interaction of the RNA polymerase flap domain with the sigma subunit in promoter recognition. *Science* 295:855–857.
4 Rao X, Deighan P, Hua Z, Hu X, Wang J, Luo M, Wang J, Liang Y, Zhong G, Hochschild A, Shen L (2009) A regulator from *Chlamydia trachomatis* modulates the activity of RNA polymerase through direct interaction with the beta subunit and the primary sigma subunit. *Genes Dev* 23:1818–1829.
5 Dove SL, Huang FW, Hochschild A (2000) Mechanism for a transcriptional activator that works at the isomerization step. *Proc Natl Acad Sci USA* 97:13215–13220.